The effect of Ge content on structural evolution of Ge-rich GeSbTe alloys at increasing temperature

L Prazakova, E Nolot, E Martinez, D Rouchon, F Fillot, N Bernier, R Elizalde, M Bernard, Gabriele Navarro

The Effect of Ge Content on Structural Evolution of Ge-rich GeSbTe Alloys at Increasing Temperature

L. Prazakova, E. Nolot*, E. Martinez, D. Rouchon, F. Fillot,
N. Bernier, R. Elizalde, M. Bernard, G. Navarro*

Univ. Grenoble Alpes, CEA, LETI, F-38000 Grenoble, France.
*contact authors: emmanuel.nolot@cea.fr, gabriele.navarro@cea.fr

Abstract

The material engineering of GeSbTe alloys has led to the significant improvements of thermal stability, necessary to ensure the data retention of the Phase-Change Memory device (PCM) over extended temperature range. However, despite the proven benefits of Ge enrichment of GeSbTe alloys, the effect of Ge content on the structure and its evolution as a function of annealing temperature remains unclear. In this paper, we present the structural analyses of as-deposited and annealed Ge-rich GeSbTe, considering the Ge enrichment (15 – 55 at. %) of $Ge_2Sb_2Te_5$ reference alloy. Based on the combination of Raman spectroscopy and X-ray diffraction techniques, we describe the progressive reorganization of the main structural features common to all investigated compositions. Therefore, we present a model describing the overall crystallization dynamics in Ge-rich GeSbTe. We highlight several competing phenomena in the system at increasing temperature, such as Ge diffusion and segregation as well as nucleation and growth of GeSbTe and Ge phases, which depends on Ge content. Our results contribute to the understanding of the crystallization mechanisms in Ge-rich GeSbTe alloys, unveiling the primary structural reorganization and crystallization of the GeSbTe phase followed by the crystallization of the Ge phase.

Keywords:
Phase change memories, Structural evolution, Raman spectroscopy, X-Ray diffraction

1 Introduction

GeSbTe alloys (GST) have been drawing attention over the last decades for their unique phase-change properties, in particular once integrated in Phase-Change Memory devices (PCM). Indeed, GeSbTe chalcogenides feature a reversible transition in temperature between the amorphous and the crystalline phase, used respectively as the high resistance state and the low resistance state in a memory device [1].
The $Ge_2Sb_2Te_5$ compound (GST225) is considered a reference alloy, since already used in optical memory applications [2,3] As regards the structure and crystallization mechanism, GST225 has been largely studied, pointing out its crystallization to metastable cubic structure (fcc) at ~160 °C and further to stable hexagonal structure (hex) at ~350 °C [4]. In recent years, the quest to improve the thermal stability of PCM led to the engineering of the alloy stoichiometry. Consequently, Ge-rich GST alloys were developed, demonstrating the ability to ensure the PCM device data retention in extended temperature range [5–9]. Previous works evidenced the increase of the crystallization temperature with increasing Ge content, as well as the GST and Ge phase segregation, which occurs at high temperatures and during the device operations [9,10]. Transmission electron microscopy (TEM) analyses were used to study the dynamics of the segregation process for a specific Ge-rich GST alloy, detecting the formation

of the Ge crystalline phase prior to a detectable GST phase [11,12]. However, in order to appreciate the fine structural evolutions of the material, a methodology based on the combination of X-ray diffraction (XRD) analysis and Raman spectroscopy can be applied. The combination of these techniques was used to investigate the phase segregation and to demonstrate the GST phase preferential crystallization in Ge-rich GeTe/SbTe-based alloys [13]. Moreover, the methodology was also used to describe the dynamics of the structural evolution of undoped and N-doped Ge-rich GST alloys as a function of temperature, showing the sequence of the main structural reorganization (i.e. Ge-Te, Sb-Te, a-Ge, etc.) [14]. The Ge enrichment of GST alloys is known to be beneficial to the thermal stability of the amorphous layer; however, a clear understanding of the impact of the Ge content on the structure of the alloys and its evolution in temperature is still missing.
In this paper, we investigate the impact of Ge content in Ge-rich GST alloys by the combination of XRD and Raman spectroscopy analyses, further supported by complementary Transmission Electron Microscopy with Energy Dispersive X-ray spectrometry (TEM-EDX) measurements. Based on our findings, we elaborate a model describing the dynamics of the structural reorganization, phase segregation and crystallization in Ge-rich GST alloys in temperature, and its dependence on Ge content.

2 Experimental Methods

Ge-rich GST layers were deposited on 200 nm Si (100) wafers by magnetron co-sputtering from $Ge_2Sb_2Te_5$ and Ge targets in Ar atmosphere and at room temperature. The thickness of deposited layers is 100 nm. The layers are protected by 3.5 nm-thick carbon capping layer deposited in-situ without air exposure to prevent layer surface oxidation. The target Ge enrichment in the deposited layers ranges from 15 at. % to 55 at. %. In the following, we will address the layers as Ge_xGST with x representing the Ge enrichment. The composition of the layers was measured by Wavelength Dispersive X-Ray Fluorescence Spectroscopy (WDXRF Rigaku AZX 400) using the methodology described in [15].
The as-deposited samples were annealed at different temperatures ranging from 200 °C to 450 °C. The ex-situ annealing was performed with a ramp-up of 10 °C/min and the samples were annealed for the duration of 5 minutes at the target temperature under inert N_2 atmosphere. Raman spectra of as-deposited and annealed samples were measured at room temperature with a 532 nm laser diode excitation source (Renishaw InVia). The measurements were performed in the range of the Raman shift from 100 cm^{-1} to 1000 cm^{-1}. The laser intensity was kept at low level to avoid the heating and hence the induced modification of the layer morphology. X-ray diffraction (XRD) data were obtained at room temperature with a two-circle diffractometer (PANanalytical Empyrean). The Cu Kα radiation (λ = 1.5406 Å) was used as X-ray source. The XRD measurements were performed in Bragg-Brentano geometry within the 2θ range 22°-56° (with a step size of 0.01°). The in-situ ellipsometry (Woollam M2000) measurements on as-deposited samples were performed using the incident light in the visible range. The same ramp as in ex-situ annealing (10 °C/min) was used for the measurements. Transmission Electron Microscopy with Energy Dispersive X-ray spectrometry (TEM-EDX) measurements were performed on the Ge-rich GST layers annealed at 400 °C. The samples were prepared by Ga^+ Focused Ion Beam (FIB) milling (FEI Helios 450). Silicon oxide and tungsten protection layers were deposited to protect the regions of interest from the tails of the ion beam. The samples were observed at 200 kV using a probe corrected Titan Themis FEI microscope equipped with the Super-X detector system for EDX. The EDX mappings were obtained with the resolution of 320x900 pixels using a dwell time of 50 µs. The quantification was performed using the k factors implemented in the Bruker Esprit software.

3 Results

In this part, we first report on the as-deposited samples studied by WDXRF, ellipsometry and Raman spectroscopy. Next, we introduce the main structural features and their evolution as a function of temperature in Ge_{45}GST alloy, which is used as an example. In the third part of the results, we extend the analyses to all the studied Ge-rich GST compositions.

3.1 As-deposited Ge-rich GST layers

WDXRF quantification of the Ge, Sb and Te content in the studied Ge-rich GST layers is shown in Fig. 1. The measured values are in good agreement with the nominal ones, with the Sb over Te ratio of 0.4, as expected from the $Ge_2Sb_2Te_5$ target used for the deposition. The global Ge content in the studied alloys increases from about 20 at. % up to more than 60 at. %.

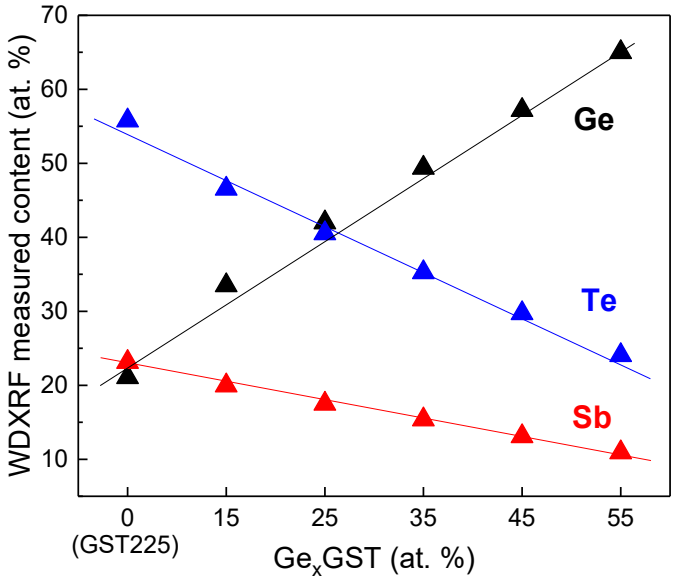

Fig. 1: Ge, Sb and Te content in studied Ge-rich GST alloys measured by WDXRF.

In-situ ellipsometry was performed in order to observe the change in optical behavior of Ge-rich GST samples with increasing temperature. Fig. 2 shows the angle psi (ψ), related to the ratio between reflection coefficient for p- and s- polarization, as a function of the annealing temperature. The GST225 sample shows two sharp increases of ψ at around ~165 °C and ~350 °C corresponding to the amorphous-to-fcc and fcc-to-hex transition, respectively. Increasing the Ge content in the layers leads to the delay of the first transition to higher temperature, whereas the fcc-to-hex transition is not observed up to 400 °C. Moreover, the global difference in ψ is reduced as the Ge content increases. In Ge_{35}GST and Ge_{45}GST, the first transition is separated into two steps, evidencing the growth of an intermediary phase in the system, which will be explained later in the text. A similar double step transition in Ge-rich GST alloys was already observed in Resistivity vs Temperature (R vs T) measurements [14]. A second sharp increase of ψ can be observed in Ge-rich GST at higher temperatures and may be attributed to the growth of the GST phase once Ge is completely segregated and starts to crystallize.

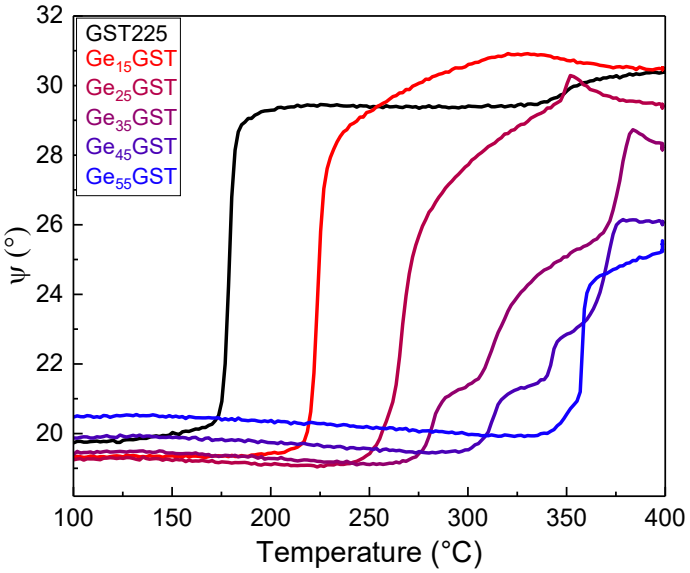

Fig. 2: In-situ ellipsometry measurements showing the delay the amorphous-to-fcc transition of GST phase and Ge phase crystallization for studied Ge-rich GST alloys.

Raman spectra of amorphous as-deposited (AD) layers are reported in Fig. 3. The spectra were normalized with regard to the intensity of the peak at 154 cm^{-1}. The spectra can be divided into two main frequency regions:

- from 100 cm^{-1} to 190 cm^{-1}, we observe several overlapping bands at ~110 cm^{-1}, 124 cm^{-1} and 154 cm^{-1}, corresponding to the different vibration modes of the GST phase [16–22]. In particular, the band at 154 cm^{-1} is assigned to the Sb-Te vibrations of $SbTe_3$ pyramidal units, the band at 124 cm^{-1} is assigned to the Ge-Te vibrations in $GeTe_{4-n}Ge_n$ (n = 1, 2) mixed tetrahedra units. The band at ~110 cm^{-1} corresponds to E_g^2 vibration of Sb-Te bonds (See Supplementary material).
- from 190 cm^{-1} to 300 cm^{-1}, two overlapping bands can be distinguished at about 270 cm^{-1} and 220 cm^{-1}. These bands are assigned to the TO and LO vibrational modes of amorphous Ge (a-Ge), respectively [23–27].

The described bands can be distinguished in the spectra of all Ge-rich GST samples. It can be noted that the band at 154 cm^{-1} assigned to the Sb-Te vibrations is stable in position and width and represents the dominant peak in the spectra, independently from the Ge content in the layer. On the contrary, the decrease in intensity of Ge-Te modes at 124 cm^{-1} and the clearer separation of the peak at 110 cm^{-1} can be observed in the alloys with higher Ge content. The intensity of the a-Ge modes increases with the Ge content in the layer, as expected.

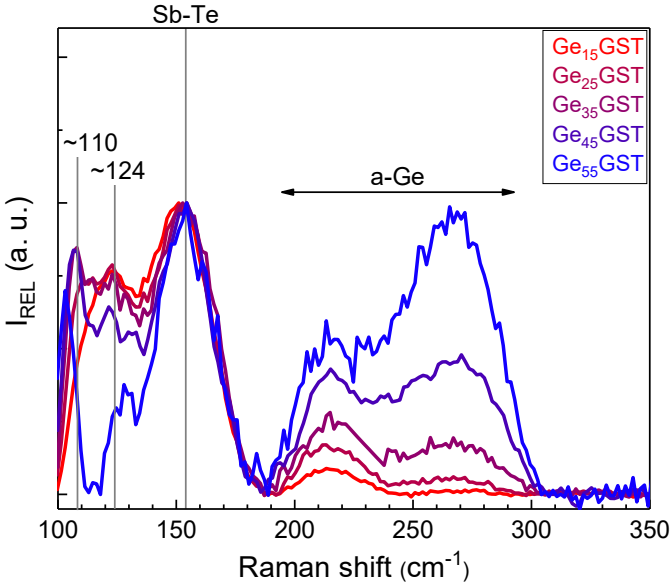

Fig. 3: Raman spectra of as-deposited Ge_xGST layers.

3.2 Evolution of Ge_{45}GST as a function of temperature

Based on the previous investigations on Ge_{45}GST alloy [14], we initially focus on this composition in order to describe the evolution of the main structural features with increasing temperature. This description will further allow to highlight the main structural changes common to all the investigated Ge-rich GST samples.

The Raman spectra in Fig. 4a evidence the stability of Sb-Te features (154 cm^{-1}) in temperature. On the contrary, the intensity of Ge-Te vibrations (124 cm^{-1}) first decreases at 300 °C and later increases at 350 °C. These changes suggest a primary reorganization of Ge-Te modes (i.e. decrease of disorder) at low annealing temperature and a further progressive rearrangement of the Ge-Te bonds around stable Sb-Te units in a GST phase. The evolution of Ge-Te features observed at 300 °C cannot be related to the appearance of a crystalline phase, as confirmed by the XRD pattern of Fig. 4b. Starting from 350 °C, the band at 100-190 cm^{-1} of the Raman spectra can be attributed to the cubic crystalline GST225 phase (GST-fcc) [14], as confirmed by XRD. At the same temperature, the a-Ge modes (190-300 cm^{-1}) are gradually reduced, turning into a narrow peak at ~300 cm^{-1}, which is assigned to the crystalline Ge mode (c-Ge) [24,27]. During the transition from a-Ge to c-Ge, an intermediary peak at ~280 cm^{-1} can be observed, which later disappears at higher temperatures. The formation of the cubic crystalline Ge phase starting from 350 °C is also confirmed by XRD. Hence, GST-fcc and Ge crystalline phases separate and further grow independently. The feature at ~30.5° in the XRD pattern at 350 °C is assigned to the formation of a transient GeSbTe phase (called G^+GST) with higher Ge content with respect to GST225. This transient phase represents a mandatory step between the starting amorphous composition, which is homogeneous and highly enriched in Ge content, and the completely segregated GST-fcc and Ge phases [14].

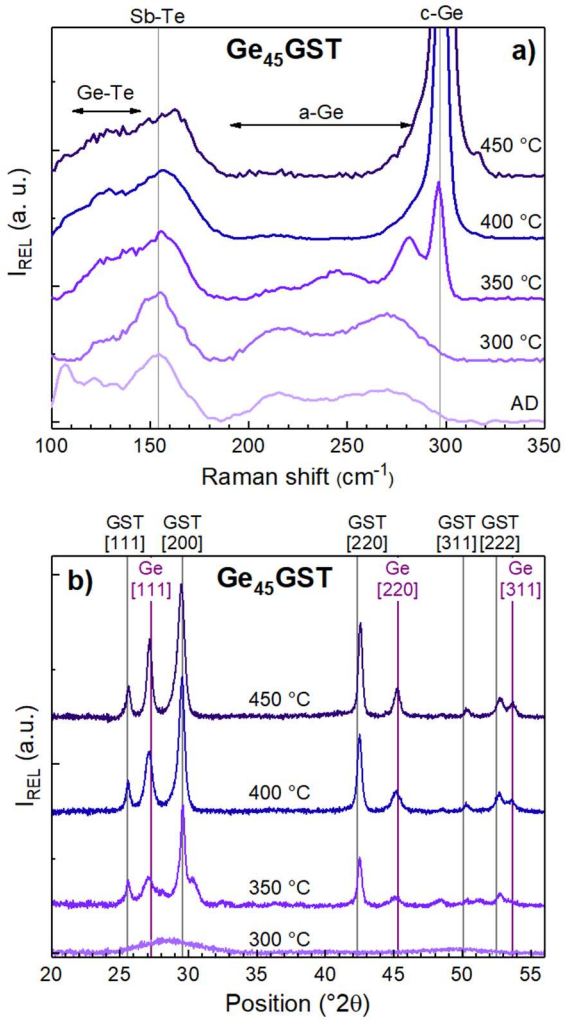

Fig. 4: Raman spectra (a) and XRD patterns (b) of as-deposited (AD) and annealed $Ge_{45}GST$. Indexation of XRD patterns is performed based on database data for cubic crystalline Ge and GST225-fcc phases (ICDD PDF Nos. 00-054-0484 and 00-004-0545).

3.3 Structural evolution of the Ge_xGST as a function of Ge enrichment and temperature

Fig. 5 shows the Raman spectra of the annealed Ge_xGST layers. The intensity of Raman spectra was normalized with regard to the intensity of the peak at 154 cm^{-1}, as previously shown for $Ge_{45}GST$. Indeed, this well-defined peak assigned to the Sb-Te vibrations is present in all the spectra at all different annealing temperatures.

In the spectra of $Ge_{15}GST$, $Ge_{25}GST$ and $Ge_{35}GST$ at 300 °C, the broad band below 190 cm^{-1} (Sb-Te and Ge-Te vibrations of a GST phase) already corresponds to that of cubic GST225. This likely indicates that the Ge-Te bond rearrangement around Sb-Te units in the layer structure is highly advanced or even completed. On the contrary, the intensity of Ge-Te modes in $Ge_{45}GST$ and $Ge_{55}GST$ is significantly lower, indicating that the structure is still disordered. The a-Ge modes (190-300 cm^{-1}) present in all compositions imply that the Ge in the layer still remains in the amorphous phase.

At the annealing temperature of 350 °C, the Ge-Te modes reorganization can already be observed in all compositions. Moreover, the peak at 110 cm^{-1}, observed at lower temperatures, completely disappears. The most significant changes occur in the region of a-Ge modes, where the c-Ge mode appears in all the spectra except for $Ge_{35}GST$. The intensity of c-Ge mode varies with the Ge content in the layer. In $Ge_{35}GST$, however, the intermediary peak at 280 cm^{-1} can

be found, corresponding to the one previously observed in $Ge_{45}GST$. Layers annealed at 400 °C and 450 °C show a good match between the spectra of all compositions. The intensity of c-Ge peak increases with the Ge content. Slight asymmetry and hence the position shift of the GST phase broad band (100-190 cm^{-1}) in the spectra at 450 °C is due to the presence of an additional low intense contribution at ~170 cm^{-1}. This contribution could be related to the rising transition of the GST225 cubic phase towards the hexagonal phase [22,28].

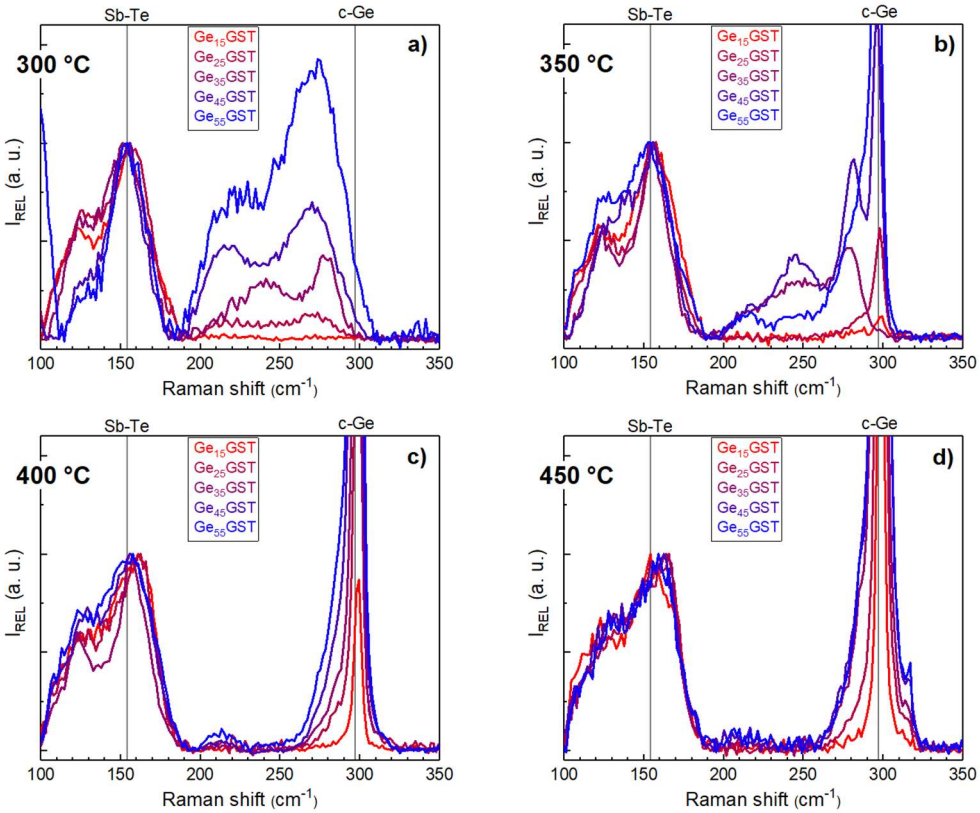

Fig. 5: Raman spectra of Ge_xGST layers annealed at 350 °C (a), 350 °C (b), 400 °C (c) and 450 °C (d).

The XRD patterns of the studied layers are presented in Fig. 6. The peak intensity in all patterns was normalized with regard to the dominant peak of the GST phase (i.e. GST[200] peak). The XRD patterns of the layers annealed at 300 °C (Fig. 6a) show the presence of the cubic GST225 (GST-fcc) crystalline phase for $Ge_{15}GST$, $Ge_{25}GST$ and $Ge_{35}GST$, while the XRD patterns of $Ge_{45}GST$ and $Ge_{55}GST$ show only a broad feature indicating a still disordered structure. The peaks in XRD patterns at 350 °C (Fig. 6b) evidence the already developed GST-fcc phase in all the compositions. Moreover, the second set of peaks, assigned to the Ge cubic crystalline phase, can be observed in all the patterns except for the $Ge_{35}GST$ composition. These observations are in good agreement with the Raman analyses. Furthermore, the broad band at ~30.5°, alongside the dominant GST[200] peak, is observed in the pattern of $Ge_{35}GST$ at 300 °C. This band is assigned to G^+GST transient phase and disappears at higher temperature. The same phenomenon was observed in $Ge_{45}GST$ at 350 °C. These findings are compatible with the ellipsometry results, evidencing an intermediary transition along the increasing ψ values (Fig. 2). The XRD patterns at 400 °C and 450 °C show the continuous intensity increase and narrowing of the GST-fcc and Ge cubic peaks indicating the crystal growth of the separated GST-fcc and Ge phases.

In $Ge_{15}GST$ and $Ge_{25}GST$, high annealing temperature further induces the intensity increase of the peaks corresponding to the GST[111] and GST[222] planes, which indicates the preferential

crystallization of the GST-fcc phase in these planes. XRD pattern of $Ge_{15}GST$ at 450 °C also evidences the significant position shift of the GST[200] and GST[220] peaks and the appearance of several new broad bands. These changes may indicate the advancing fcc-to-hex phase evolution of GST225 (GST225-hex: PDF No. 04-008-1147), or much more likely the vacancies reordering in the cubic phase, which occurs well before the fcc-to-hex transition [29].

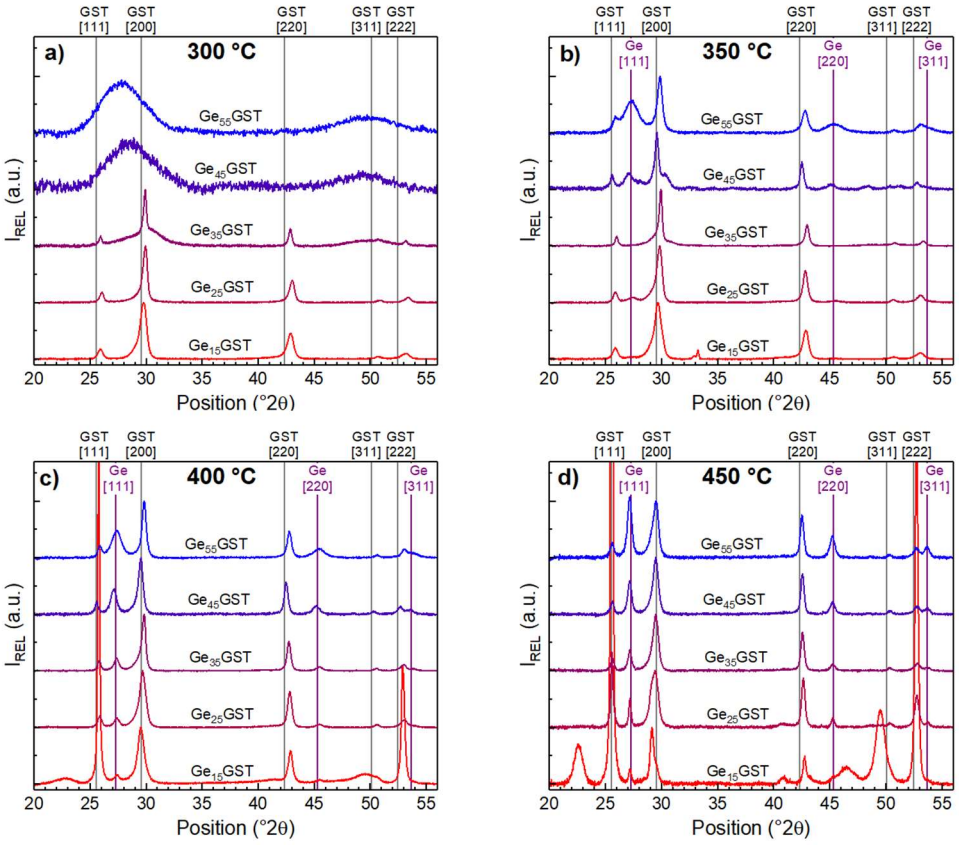

Fig. 6: XRD patterns of Ge_xGST layers annealed at 300 °C (a), 350 °C (b), 400 °C (c), and 450 °C (d).

4 Discussion

Raman spectra of as-deposited amorphous Ge-rich GST layers feature the vibrational modes of the GST phase and the a-Ge phase. In particular, the main band of all spectra is assigned to the vibrations of Sb-Te units characteristic for the GST phase and remains stable up to high annealing temperatures (Fig. 5). On the contrary, we can observe changes in the intensity of Ge-Te modes with temperature, indicating the ongoing Ge-Te bonds rearrangement around Sb-Te units. In $Ge_{15}GST$, $Ge_{25}GST$ and $Ge_{35}GST$ such rearrangement leads to the formation of the crystalline GST-fcc phase at 300 °C (Fig. 6). In $Ge_{45}GST$ and $Ge_{55}GST$, however, the formation of the crystalline GST-fcc phase is delayed to 350 °C. At 350 °C, the coexistence of both GST-fcc and Ge crystalline phases is observed (Fig. 6), which demonstrates that the Ge phase segregation already started. $Ge_{35}GST$ is the only sample not showing the Ge crystalline phase at 350 °C, however, we can recognize the already advanced evolution of a-Ge modes (i.e. ordering) through the appearance of the intermediary peak at 280 cm^{-1} (Fig. 5). These observations highlight the existing competition/concurrence of the following phenomena, which depend on Ge content in the layer and on temperature:

a) the nucleation and growth of a GST phase (i.e. GST225-fcc);

b) the Ge segregation out of the formed GST phase, which is delayed by increasing Ge content (i.e. lower diffusivity), but favored by increasing temperature (i.e. higher diffusivity of Ge);
c) the backward chemical diffusion of Ge (hinders the GST phase formation), which increases with Ge content;
d) the nucleation and growth of Ge crystalline phase (favors the Ge segregation).

This model, presenting the several phenomena, shows that the segregation of the different phases is initiated by the reorganization driven by the stable Sb-Te units in GST phase and by the consequent nucleation of a GST phase. In $Ge_{35}GST$, the balance between Ge (~50 at. %) and Sb/Te content likely delays the formation of the Ge crystalline phase due to the competition between delayed Ge segregation and enhanced Ge backward diffusion. Indeed, the Ge segregation is greatly disfavored by high Ge content in $Ge_{45}GST$ and $Ge_{55}GST$, which can explain the observed delay of the GST phase crystallization to 350 °C.
Fig. 7 shows the values of peak broadening at full width at half maximum intensity (FWHM) for GST[220] and Ge[111] peaks and the calculated crystallites sizes of each phase. The FWHM parameter here represents the line broadening of the peak after subtracting the instrumental contribution. The crystallites size of the GST-fcc and Ge phases was calculated using the Scherer equation. For both GST-fcc and Ge phases we can observe the decrease of FWHM, i.e. increase of crystallites size with temperature, thus indicating a strong correlation between the phases' crystalline growth. On the contrary, there is no evident dependence on Ge content. It is interesting to notice that the GST-fcc crystallites size is larger than the equivalent Ge crystal size at all compositions. The crystallites size of both phases reaches similar values at 450 °C, independently from the Ge content in the layer. This result supports previous discussions about primary nucleation and crystalline growth of GST phase and consequent crystalline growth of the Ge phase, which is very fast at high temperatures. Fig. 7 also highlights the crystallization temperature of a-Ge reduced below 350 °C, whereas it is generally reported to be in the range of 480 °C – 530 °C [30–33]. Indeed, the heterogeneous nucleation of Ge can be likely observed in our samples, which is induced at the interfaces of the already existing GST crystalline seeds [34–36].

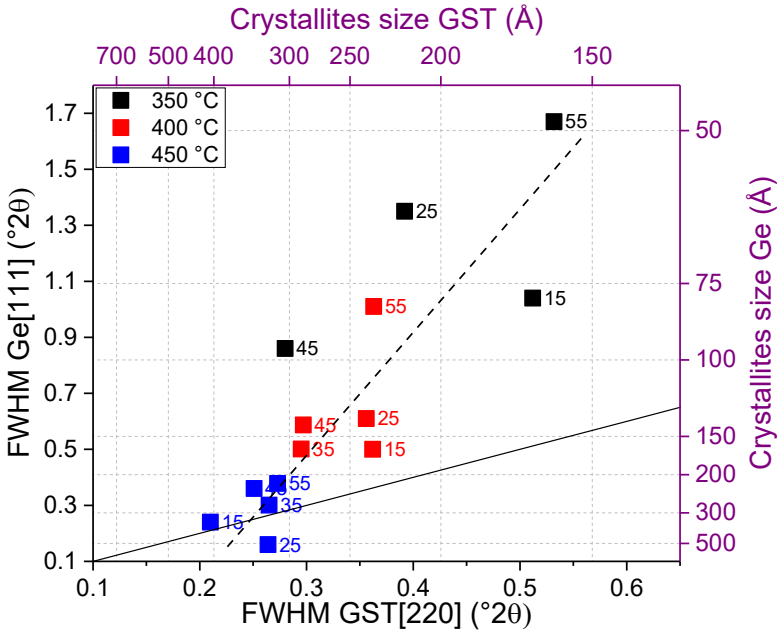

Fig. 7: Correlation of the FWHM and crystallites sizes for the GST225-fcc phase and Ge crystalline phases (dashed line). The values were taken from the GST[220] and Ge[111] peaks. The solid line represents the 1:1 ratio between the crystallites size of both phases.

The progression of GST crystallization followed by Ge crystallization is well observable in particular in the Ge_xGST layers with low Ge enrichment, in which the two phases appear at different annealing temperatures (Fig. 6). On the contrary, the GST and Ge crystalline phases appear at the same annealing temperature in the Ge-rich GST layers with higher Ge enrichment, which results from two concurrent phenomena: delayed GST phase crystallization and high crystalline growth speed of Ge phase.

The dynamics of the GST crystallization and Ge segregation processes can be well observed in the case of $Ge_{35}GST$. XRD patterns of $Ge_{35}GST$ at 300 °C, 350 °C and 400 °C without normalization are shown in Fig. 8. The measurement parameters were kept the same during the acquisition, which allows us to compare the peak intensity of the emerging GST-fcc phase. The XRD pattern at 300 °C shows the peak GST[200] together with the broad band of the transient phase G^+GST at ~30.5°. The low intense but narrow peak of GST[200] indicates the formation of high quality grains though present in small quantity, which are enclosed in a disordered Ge enriched G^+GST phase. High Ge content and relatively low temperature do not yet allow the system to expulse abundant Ge and therefore completely separate the Ge and GST-fcc phases. Increasing the annealing temperature up to 350 °C, the Ge diffusivity and hence the Ge expulsion from G^+GST are enhanced. This process leads to the gradual disappearance of the transient G^+GST phase and to the progressive definition of GST polycrystalline and Ge crystalline regions. This is evidenced in the XRD pattern at 350 °C as the intensity of the GST[200] peak increases and the peak becomes slightly broader than at 300 °C. The broad feature assigned to G^+GST is then reduced in intensity. XRD pattern at 400 °C further confirms the complete disappearance of G^+GST phase, whilst the separated Ge phase appears (Ge[111] peak), enhanced by the heterogeneous nucleation and high growth speed at the interface with the already formed GST-fcc phase. The model is represented schematically in Fig. 9.

The difficulty to observe such transient phenomena in Ge_xGST layers with lower Ge contents is likely related to the reduced formation of the region enriched in Ge, which surrounds the GST-fcc nuclei. Lowering the Ge content likely reduces the time scale for observing the broad band as well as its intensity.

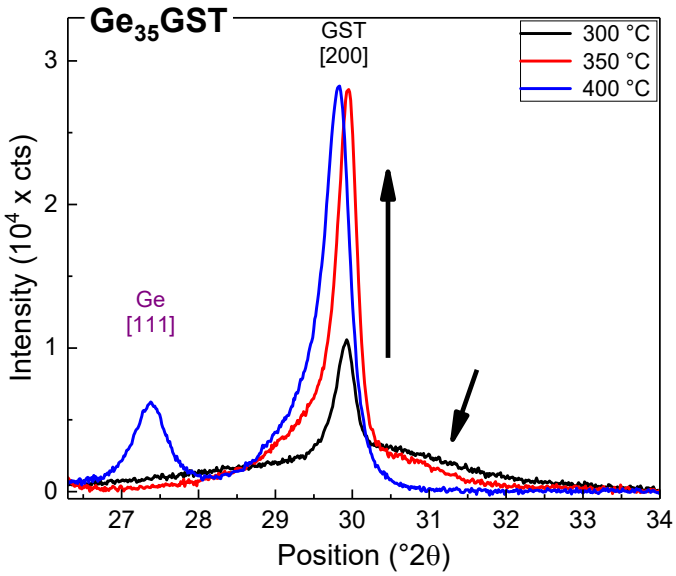

Fig. 8: XRD patterns (range 26°-34°) for $Ge_{35}GST$ alloy at 300 °C, 350 °C and 400 °C highlighting the intensity increase of the GST[200] peak related to the GST225-fcc phase and the reduction of the broad band assigned to transient G^+GST phase.

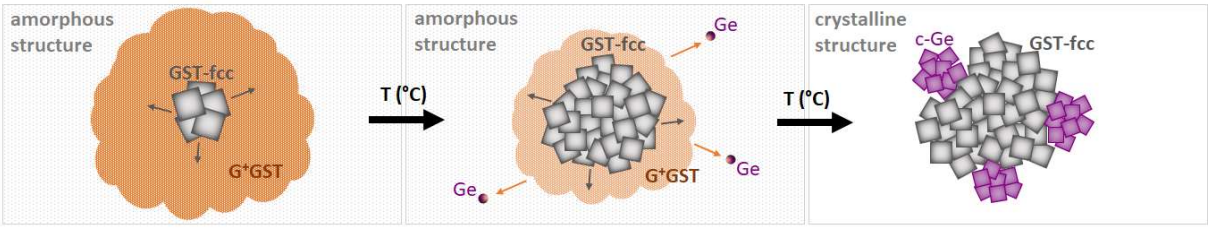

Fig. 9: Scheme representing the progress of GST225-fcc phase crystallization, disappearance of transient $G^{+}GST$ phase with the expulsion of Ge atoms and following Ge phase crystallization with increasing annealing temperature.

In order to follow the progress of the demixing process in the alloy, TEM images with EDX analyses were performed on Ge_xGST layers annealed at 400 °C. The Ge and Te cartographies in Fig. 10a show the formation of Ge-rich and Te-rich regions indicating the complete segregation of GST and Ge phases. This findings confirm the XRD results (Fig. 6), where the already developed GST-fcc and Ge cubic crystalline phase are observed. Moreover, the cartographies show the dominance of the Ge phase with increasing Ge content, as expected. Based on the data extracted from EDX analyses, we reconstructed the compositional distribution of phases present along the tie line between GST225 phase and pure Ge phase. The cartographies shown in Fig. 10b demonstrate the distribution from highly occurred phase to less occurred phase (i.e. transition from dark to light zones, respectively) for the studied alloys. We can clearly observe the gradual transition of the distribution towards the pure Ge phase as the Ge content in the layers increases. This transition suggests the progressive tendency of the pure Ge phase to dominate the system dynamics, which is in good agreement with our XRD results.

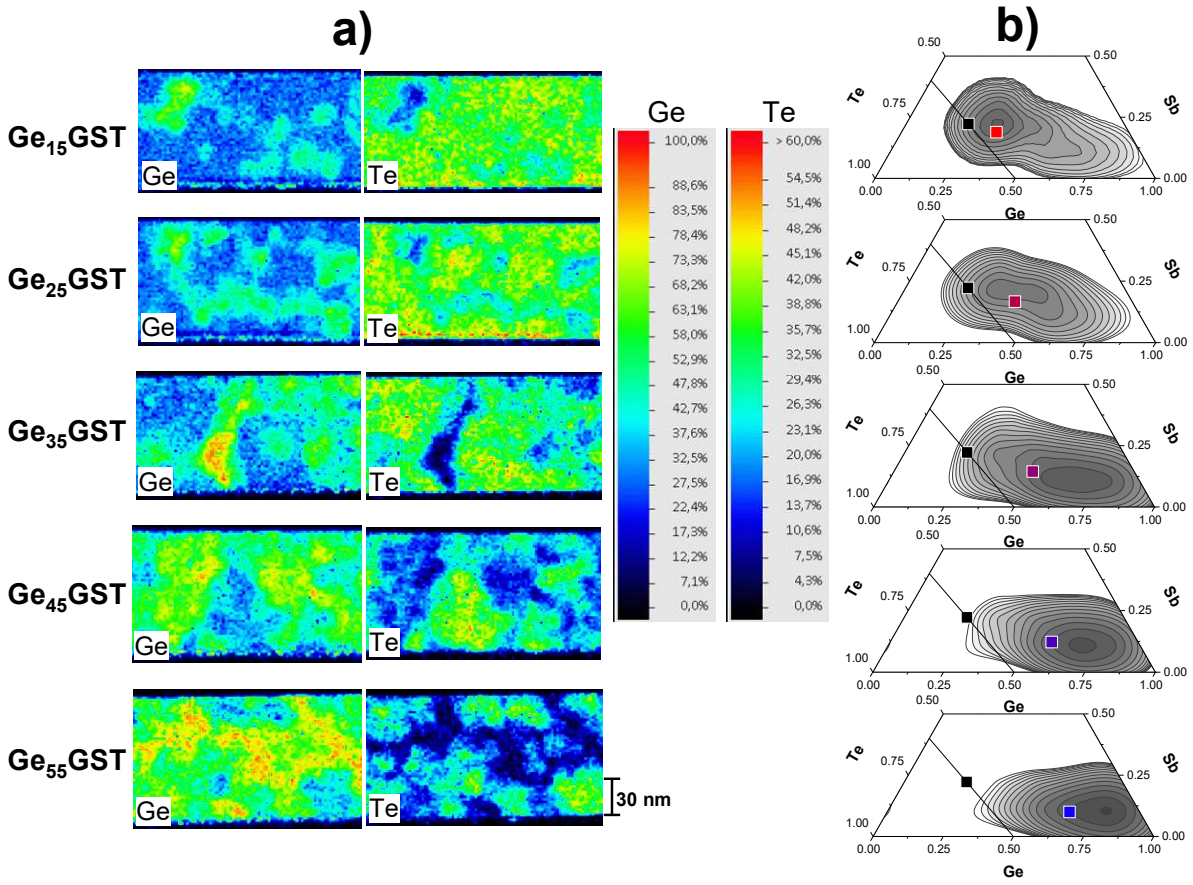

Fig. 10 : TEM-EDX analyses on Ge_xGST layers annealed at 400 °C. a) Ge an Te cartographies highlighting the elemental migration; b) Ge-Sb-Te ternary diagram showing the compositional distribution along the tie line

between GST225 (black square) and pure Ge phase (right bottom corner of the ternary diagram). The colored squares represent the position of corresponding Ge_xGST.

5 Conclusions

The crystallization dynamics of the Ge-rich GST alloys with a large range of Ge enrichment were investigated by Raman spectroscopy and XRD. Combining the results from the two characterization techniques we observe that the structural evolution process in temperature begins with the Ge-Te bond rearrangement around stable Sb-Te units characteristic of GST phase, independently from the Ge content in the alloy. Our results further support the primary crystallization of GST-fcc phase, followed by the heterogeneous nucleation and consequent growth of Ge phase. We show that the crystallites sizes of the GST-fcc and Ge phases are strongly correlated and increase with annealing temperature, independently from Ge content in the alloy. We present a model taking into account several phenomena, which occur during the structural evolution of the alloys and which are delayed to higher temperature as the Ge content increases. Besides, the model includes the experimentally observed transient G^+GST phase. The GST phase crystallization followed by the Ge phase crystallization are well observed in layers with low Ge content since they appear at different temperatures. On the contrary, these two processes appear simultaneously at high temperature in the layers with high Ge content, resulting from delayed GST phase crystallization and fast Ge crystal growth. These findings contribute to the long-lasting discussions on the crystallization mechanism of Ge-rich GST alloys.

Acknowledgments

This work has been performed with the help of the NanoCaracterization Platform of Minatec with the financial support of the "Recherche Technologique de Base" program. It has been partially supported by the European 783176 WAKeMeUP Project, financed by European commission, French government and Auvergne-Rhône Alpes Region.

Supplementary materials

See the Supplementary material for the extended analyses of Raman spectra of as-deposited and annealed (350 °C) $Ge_{15}GST$, $Ge_{35}GST$ and $Ge_{55}GST$ alloys.

Data Availability

The data that support the findings of this study are available from the corresponding authors upon reasonable request.

References

[1] S. Raoux, W. Wełnic, D. Ielmini, Phase Change Materials and Their Application to Nonvolatile Memories, Chem. Rev. 110 (2010) 240–267. https://doi.org/10.1021/cr900040x.

[2] N. Yamada, E. Ohno, K. Nishiuchi, N. Akahira, M. Takao, Rapid-phase transitions of GeTe-Sb $_2$ Te $_3$ pseudobinary amorphous thin films for an optical disk memory, Journal of Applied Physics. 69 (1991) 2849–2856. https://doi.org/10.1063/1.348620.

[3] A. Redaelli, ed., Phase Change Memory, Springer International Publishing, Cham, 2018. https://doi.org/10.1007/978-3-319-69053-7.

[4] I. Friedrich, V. Weidenhof, W. Njoroge, P. Franz, M. Wuttig, Structural transformations of Ge2Sb2Te5 films studied by electrical resistance measurements, Journal of Applied Physics. 87 (2000) 4130–4134. https://doi.org/10.1063/1.373041.

[5] H.Y. Cheng, J.Y. Wu, R. Cheek, S. Raoux, M. BrightSky, D. Garbin, S. Kim, T.H. Hsu, Y. Zhu, E.K. Lai, E. Joseph, A. Schrott, S.C. Lai, A. Ray, H.L. Lung, C. Lam, A thermally robust phase change memory by engineering the Ge/N concentration in (Ge, N)xSbyTe z phase change material, in: 2012 International Electron Devices Meeting, IEEE, San Francisco, CA, USA, 2012: p. 31.1.1-31.1.4. https://doi.org/10.1109/IEDM.2012.6479141.

[6] S.M.S. Privitera, V. Sousa, C. Bongiorno, G. Navarro, C. Sabbione, E. Carria, E. Rimini, Atomic diffusion in laser irradiated Ge rich GeSbTe thin films for phase change memory applications, J. Phys. D: Appl. Phys. 51 (2018) 145103. https://doi.org/10.1088/1361-6463/aab1d0.

[7] E. Palumbo, P. Zuliani, M. Borghi, R. Annunziata, Forming operation in Ge-rich Ge x Sb y Te z phase change memories, Solid-State Electronics. 133 (2017) 38–44. https://doi.org/10.1016/j.sse.2017.03.016.

[8] G. Navarro, G. Bourgeois, J. Kluge, A.L. Serra, A. Verdy, J. Garrione, M.-C. Cyrille, N. Bernier, A. Jannaud, C. Sabbione, M. Bernard, E. Nolot, F. Fillot, P. Noe, L. Fellouh, G. Rodriguez, V. Beugin, O. Cueto, N. Castellani, J. Coignus, V. Delaye, C. Socquet-Clerc, T. Magis, C. Boixaderas, S. Barnola, E. Nowak, Phase-Change Memory: Performance, Roles and Challenges, in: 2018 IEEE International Memory Workshop (IMW), IEEE, Kyoto, 2018: pp. 1–4. https://doi.org/10.1109/IMW.2018.8388845.

[9] P. Zuliani, E. Varesi, E. Palumbo, M. Borghi, I. Tortorelli, D. Erbetta, G.D. Libera, N. Pessina, A. Gandolfo, C. Prelini, L. Ravazzi, R. Annunziata, Overcoming Temperature Limitations in Phase Change Memories With Optimized ${\rm Ge}_{\rm x}{\rm Sb}_{\rm y}{\rm Te}_{\rm z}$, IEEE Transactions on Electron Devices. 60 (2013) 4020–4026. https://doi.org/10.1109/TED.2013.2285403.

[10] V. Sousa, G. Navarro, N. Castellani, M. Coue, O. Cueto, C. Sabbione, P. Noe, L. Perniola, S. Blonkowski, P. Zuliani, R. Annunziata, Operation fundamentals in 12Mb Phase Change Memory based on innovative Ge-rich GST materials featuring high reliability performance, in: IEEE, 2015: pp. T98–T99. https://doi.org/10.1109/VLSIT.2015.7223708.

[11] M. Agati, F. Renaud, D. Benoit, A. Claverie, In-situ transmission electron microscopy studies of the crystallization of N-doped Ge-rich GeSbTe materials, MRC. 8 (2018) 1145–1152. https://doi.org/10.1557/mrc.2018.168.

[12] M. Agati, M. Vallet, S. Joulié, D. Benoit, A. Claverie, Chemical phase segregation during the crystallization of Ge-rich GeSbTe alloys, J. Mater. Chem. C. 7 (2019) 8720–8729. https://doi.org/10.1039/C9TC02302J.
[13] F. Di Biagio, S. Cecchi, F. Arciprete, R. Calarco, Crystallization Study of Ge-Rich $(GeTe)_m(Sb_2Te_3)_n$ Using Two-Step Annealing Process, Phys. Status Solidi RRL. 13 (2019) 1800632. https://doi.org/10.1002/pssr.201800632.
[14] L. Prazakova, E. Nolot, E. Martinez, F. Fillot, D. Rouchon, N. Rochat, M. Bernard, C. Sabbione, D. Morel, N. Bernier, A. Grenier, A.-M. Papon, M.-C. Cyrille, G. Navarro, Temperature driven structural evolution of Ge-rich GeSbTe alloys and role of N-doping, Journal of Applied Physics. 128 (2020) 215102. https://doi.org/10.1063/5.0027734.
[15] C. Jeynes, E. Nolot, C. Costa, C. Sabbione, W. Pessoa, F. Pierre, A. Roule, G. Navarro, M. Mantler, Quantifying nitrogen in GeSbTe:N alloys, J. Anal. At. Spectrom. 35 (2020) 701–712. https://doi.org/10.1039/C9JA00382G.
[16] K.S. Andrikopoulos, S.N. Yannopoulos, G.A. Voyiatzis, A.V. Kolobov, M. Ribes, J. Tominaga, Raman scattering study of the a-GeTe structure and possible mechanism for the amorphous to crystal transition, Journal of Physics: Condensed Matter. 18 (2006) 965–979. https://doi.org/10.1088/0953-8984/18/3/014.
[17] K.S. Andrikopoulos, S.N. Yannopoulos, A.V. Kolobov, P. Fons, J. Tominaga, Raman scattering study of GeTe and Ge2Sb2Te5 phase-change materials, Journal of Physics and Chemistry of Solids. 68 (2007) 1074–1078. https://doi.org/10.1016/j.jpcs.2007.02.027.
[18] P. Němec, A. Moreac, V. Nazabal, M. Pavlišta, J. Přikryl, M. Frumar, Ge–Sb–Te thin films deposited by pulsed laser: An ellipsometry and Raman scattering spectroscopy study, Journal of Applied Physics. 106 (2009) 103509. https://doi.org/10.1063/1.3259435.
[19] G.C. Sosso, S. Caravati, R. Mazzarello, M. Bernasconi, Raman spectra of cubic and amorphous Ge 2 Sb 2 Te 5 from first principles, Phys. Rev. B. 83 (2011) 134201. https://doi.org/10.1103/PhysRevB.83.134201.
[20] S. Caravati, M. Bernasconi, T.D. Kühne, M. Krack, M. Parrinello, Coexistence of tetrahedral- and octahedral-like sites in amorphous phase change materials, Applied Physics Letters. 91 (2007) 171906. https://doi.org/10.1063/1.2801626.
[21] R. Mazzarello, S. Caravati, S. Angioletti-Uberti, M. Bernasconi, M. Parrinello, Signature of Tetrahedral Ge in the Raman Spectrum of Amorphous Phase-Change Materials, Physical Review Letters. 104 (2010). https://doi.org/10.1103/PhysRevLett.104.085503.
[22] L. Bo, S. Zhi-Tang, Z. Ting, F. Song-Lin, C. Bomy, Raman spectra and XPS studies of phase changes in $Ge_2Sb_2Te_5$ films, Chinese Phys. 13 (2004) 1947–1950. https://doi.org/10.1088/1009-1963/13/11/033.
[23] I. Chambouleyron, F. Marques, J. Cisneros, F. Alvarez, S. Moehlecke, W. Losch, I. Pereyra, Optical properties of non-stoichiometric germanium nitride compounds (a-GeNx), Journal of Non-Crystalline Solids. 77–78 (1985) 1309–1312. https://doi.org/10.1016/0022-3093(85)90899-3.
[24] P. Kazimierski, J. Tyczkowski, M. Kozanecki, Y. Hatanaka, T. Aoki, Transition from Amorphous Semiconductor to Amorphous Insulator in Hydrogenated Carbon−Germanium Films Investigated by Raman Spectroscopy, Chemistry of Materials. 14 (2002) 4694–4701. https://doi.org/10.1021/cm020428s.
[25] H. Jamali, R. Mozafarinia, A. Eshaghi, Evaluation of chemical and structural properties of germanium-carbon coatings deposited by plasma enhanced chemical vapor deposition, Journal of Alloys and Compounds. 646 (2015) 360–367. https://doi.org/10.1016/j.jallcom.2015.06.091.
[26] J.S. Lannin, N. Maley, S.T. Kshirsagar, Raman scattering and short range order in amorphous germanium, Solid State Communications. 53 (1985) 939–942. https://doi.org/10.1016/0038-1098(85)90464-8.
[27] H. Jamali, R. Mozafarinia, A. Eshaghi, The effect of carbon content on the phase structure of amorphous/nanocrystalline Ge 1−x C x films prepared by PECVD, Surface and Coatings Technology. 310 (2017) 1–7. https://doi.org/10.1016/j.surfcoat.2016.12.043.
[28] Z. Xu, C. Chen, Z. Wang, K. Wu, H. Chong, H. Ye, Optical constants acquisition and phase change properties of $Ge_2Sb_2Te_5$ thin films based on spectroscopy, RSC Adv. 8 (2018) 21040–21046. https://doi.org/10.1039/C8RA01382A.
[29] J.-J. Wang, Y.-Z. Xu, R. Mazzarello, M. Wuttig, W. Zhang, A Review on Disorder-Driven Metal–Insulator Transition in Crystalline Vacancy-Rich GeSbTe Phase-Change Materials, Materials. 10 (2017) 862. https://doi.org/10.3390/ma10080862.
[30] A.F. Khan, M. Mehmood, A.M. Rana, T. Muhammad, Effect of annealing on structural, optical and electrical properties of nanostructured Ge thin films, Applied Surface Science. 256 (2010) 2031–2037. https://doi.org/10.1016/j.apsusc.2009.09.043.
[31] Q. Tao, N. Chen, C. Wang, M. Dayan, Y. Bai, J. Chen, Characterization and mechanism of crystallization of Ge films on silicon substrate with graphite buffer layer, Materials Science in Semiconductor Processing. 84 (2018) 167–170. https://doi.org/10.1016/j.mssp.2018.05.011.
[32] F. Katsuki, K. Hanafusa, M. Yonemura, T. Koyama, M. Doi, Crystallization of amorphous germanium in an Al/a-Ge bilayer film deposited on a SiO2 substrate, Journal of Applied Physics. 89 (2001) 4643–4647. https://doi.org/10.1063/1.1359149.

[33] C.-Y. Tsao, J.W. Weber, P. Campbell, P.I. Widenborg, D. Song, M.A. Green, Low-temperature growth of polycrystalline Ge thin film on glass by in situ deposition and ex situ solid-phase crystallization for photovoltaic applications, Applied Surface Science. 255 (2009) 7028–7035. https://doi.org/10.1016/j.apsusc.2009.03.035.
[34] E. Carria, A.M. Mio, S. Gibilisco, M. Miritello, C. Bongiorno, M.G. Grimaldi, E. Rimini, Amorphous-Crystal Phase Transitions in $Ge_x Te_{1-x}$ Alloys, Journal of The Electrochemical Society. 159 (2011) H130–H139. https://doi.org/10.1149/2.048202jes.
[35] A. Debunne, K. Virwani, A. Padilla, G.W. Burr, A.J. Kellock, V.R. Deline, R.M. Shelby, B. Jackson, Evidence of Crystallization–Induced Segregation in the Phase Change Material Te-Rich GST, J. Electrochem. Soc. 158 (2011) H965. https://doi.org/10.1149/1.3614508.
[36] W. Knaepen, S. Gaudet, C. Detavernier, R.L. Van Meirhaeghe, J.J. Sweet, C. Lavoie, *In situ* x-ray diffraction study of metal induced crystallization of amorphous germanium, Journal of Applied Physics. 105 (2009) 083532. https://doi.org/10.1063/1.3110722.